THE VETMOUSETRAP™: A DEVICE FOR COMPUTED TOMOGRAPHIC IMAGING OF THE THORAX OF AWAKE CATS

CINTIA R. OLIVEIRA, FRANK N. RANALLO, GERALD J. PIJANOWSKI, MARK A. MITCHELL, MAURIA A. O'BRIEN, MAUREEN MCMICHAEL, SUSAN K. HARTMAN, JODI S. MATHESON, ROBERT T. O'BRIEN

The VetMousetrap™, a novel device that allows computed tomography (CT) of awake cats and provides a clinically supportive environment, is described. Ten normal cats were used to test the device for ambient internal oxygen, carbon dioxide levels, and temperature. Twenty-two awake normal cats were imaged using a 16-multislice helical CT unit to evaluate dose-equivalent protocols. Two different X-ray tube potentials (kV), 80 and 120, and two different helical pitches, 0.562 and 1.75, were evaluated. The signal intensity of the pulmonary parenchyma (SI_{lung}), signal intensity of background (SI_{backgr}), contrast, noise, signal-to-noise ratio (SNR), and contrast-to-noise ratio (CNR) were calculated. Three evaluators ranked the images for sharpness of liver margins, motion, helical, and windmill artifacts. CT was successfully completed in 20 of 22 cats. No artifacts directly related to the device were detected. Overall, 75 of 80 (94%) examinations were judged to have absent or minimal motion artifact. A statistically significant difference was found for SNR ($P = 0.001$) and CNR ($P = 0.001$) between all protocols. The higher pitch protocols had significantly lower noise and higher SNR and CNR, lower motion artifact but greater helical artifacts. A protocol using 80 kV, 130 mA, 0.5 s, and 0.562 pitch with 1.25 mm slice thickness, and 0.625 mm slice reconstruction interval is recommended. The VetMousetrap™ appears to provide the opportunity for diagnostic CT imaging of the thorax of awake cats. © 2010 *Veterinary Radiology & Ultrasound*

Key words: cat, computed tomography, respiratory, thorax.

Introduction

IN HUMANS, COMPUTED TOMOGRAPHY (CT) is the primary diagnostic tool for patients with clinical signs of thoracic disease.[1,2] Compared with thoracic radiography, CT images have superior contrast resolution and anatomic superposition is not a problem. Pathologic changes that are not apparent on survey radiographs may be detected using CT.[3–7,40] CT is also used to differentiate pleural, extrapleural, or mediastinal tissues from lung.[3,4] The use of CT to diagnose thoracic diseases in anesthetized cats has been described.[3–5]

In veterinary medicine, survey thoracic radiography is the standard imaging modality for evaluating the thorax.[3,8] This is due, at least in part, to the need for general anesthesia when performing CT. General anesthesia has inherent risks and causes varying degrees of atelectasis that can mimic or obscure underlying disease.[9–12] Additional scans in different positions may be necessary to evaluate the patient fully, thereby increasing imaging and anesthesia time.[13]

It would be advantageous if the benefits of CT for thoracic imaging could be applied more frequently. This is especially true with the advent of multidetector CT technology that has led to considerably decreased examination time, substantially increased longitudinal resolution by means of reduced slice thickness and slice reconstruction interval, and improved multiplanar and three-dimensional (3D) reconstruction.[14] With multidetector CT scanners, isotropic pixels allow reformatted images to have the same quality as those acquired in the plane imaged directly.[15] In pediatric CT, the high speed of multidetector CT imaging has decreased the need for sedation significantly.[16,17,41] In veterinary medicine, use of multidetector CT scanners allows the possibility to scan sedated or awake patients.

Our purposes were twofold. The first was to design a clinically supportive device that minimizes movement of awake feline patients during CT examination. We hypothesized that the device would: (1) allow CT examination of nonsedated, unanesthetized cats with minimal to no motion artifact; (2) create no CT artifact; and (3) improve the clinical environment of the imaged patient compared with radiography. The second purpose was to evaluate the impact of kV, pitch, and patient size on image quality

From the Department of Veterinary Clinical Medicine, University of Illinois at Urbana-Champaign, 1008 W. Hazelwood Dr, Urbana, IL 61802 (Oliveira, Mitchell, M. O'Brien, McMichael, Hartman, Matheson, and R. O'Brien), Department of Medical Physics, University of Wisconsin, Madison, WI 53705 (Ranallo), and Department of Veterinary Biosciences, University of Illinois at Urbana-Champaign, Urbana, IL 61802 (Pijanowski).

Presented in part at the International Veterinary Radiology Association Meeting in Búzios, Rio de Janeiro, Brazil, July of 2009.

Address correspondence and reprint requests to Cintia R. Oliveira, at the above address. E-mail: oliveir1@illinois.edu

Received May 7, 2010; accepted for publication June 8, 2010.
doi: 10.1111/j.1740-8261.2010.01726.x

during helical CT imaging of the thorax in awake cats. The initial hypotheses were as follows: (1) the protocols with lowest kV would have the best contrast; (2) the protocols with higher pitch would have less motion artifact; (3) the size, conformation, and body weight of the cat would have no impact on image quality, regardless of protocol; and (4) no pulmonary atelectasis would be detected.

Materials and Methods

There were two phases to the study. In phase 1, a device to facilitate thoracic CT imaging of awake cats, the VetMousetrap™* was designed and tested. Environmental parameters within the device, including temperature, carbon dioxide (CO_2), and oxygen levels, where measured using 10 clinically normal cats. In phase 2, the device was used to scan 22 clinically normal awake cats with four different dose-equivalent CT protocols.

Phase 1

When developing the device, both the clinical and imaging needs of patients were considered. The clinical needs required the device to: (1) allow access for oxygen administration at therapeutic levels; (2) allow access for intravenous (IV) lines without the need to disconnect the lines when placing or removing the patient from the device; (3) be symmetric, providing ports for catheter and oxygen access on both ends of the device; (4) be transparent, allowing visual observation of the patient; (5) have a closure mechanism that allowed quick removal of the patient; (6) have a secure closure mechanism preventing patient escape; (7) provide a low-heat environment; (8) avoid clinically relevant elevation of CO_2; (9) be portable; and (10) be easily disinfected.

The imaging needs were that the device: (1) have low X-ray attenuation; (2) have a symmetric, curved cross-sectional shape to avoid imaging artifacts; (3) have a narrow and short lumen to limit patient motion; (4) have no metal parts; (5) be rugged enough for daily use; and (6) allow additional padding to compensate for patients of different body sizes and behavioral characteristics.

Different material types and shapes were tested for attenuation and artifact production, and varying lengths and diameters were tested for patient compliance, ruggedness, and clinical utility.

To test the final device design for ambient internal oxygen, CO_2 levels, and temperature, 10 cats were evaluated. These were clinically healthy young adults ranging in size from 3.3 to 7 kg (mean 4.9 kg). The cats were placed inside the device and the following parameters were measured at times 0, 5, 10, 15, 20, 25, and 30 min: CO_2, fraction of inspired oxygen (FiO_2), internal chamber temperature, and subject respiratory rates. An anesthesia monitor† was used to measure the above parameters. The tubing that would normally fit onto a special cuff on the endotracheal tube was placed into one of the IV line access ports at one end of the device. The monitor recorded end-tidal CO_2 ($ETCO_2$), which was extrapolated as the CO_2 level within the device. The FiO_2 was measured via the same tubing. A probe to measure temperature was placed into one of the oxygen ports of the device. Oxygen was provided via an oxygen flow meter, with a humidifier, at a rate of 2 l/min into an oxygen port on the other end of the device. Cats were not restrained inside the device.

Phase 2

Twenty-two clinically healthy cats were imaged within the device. CT was performed without sedation or general anesthesia using a 16-slice helical CT scanner‡ and the VetMousetrap™.

The cats were placed inside the VetMousetrap™ before the CT examination. The device was secured to the CT table with standard CT table velcro straps. These also provided additional security to the top portion of the device. Supplemental foam wedges were added as necessary to encourage the cats to remain in a neutral sternal position within the device. Cats were not restrained inside the device and were monitored visually throughout the procedure. Oxygen was provided at a flow of 2 l/min for all animals during the procedure. To avoid prescan scouts, images were acquired of the entire VetMousetrap™, which resulted in a whole-body study. The CT table was kept at a predetermined height of 170 cm, and the device was always placed on a same predetermined position on the CT table. Postimage acquisition, the cats were removed from the device. Two cats exhibited signs of overt stress inside the device and were excluded from the study.

In the remaining 20 cats, two different kV settings and two different helical pitch settings were tested resulting in four dose-equivalent protocols. The goal was to test a low and a high kV (80 and 120) and two extremes of pitch (0.562 and 1.75), while keeping the CT dose index volume ($CTDI_{vol}$) of the scans constant. The scan rotation time for all imaging in this study was 0.5 s. The initial protocol was set as 80 kV, a pitch of 1.75 and 400 mA. To obtain a protocol with the same kV and a pitch of 0.562, we decreased the mA by the same factor with which we decreased the pitch (0.32), resulting in 128 mA. Thus, both protocols had the same effective mAs (mA × rotation time/pitch) of 114. To change the kV, we used information from the technical data sheet of the CT scanner.§ According to

*University of Illinois at Urbana-Champaign, Urbana, IL.

†Datascope Mindray DS USA Inc., Mahwah, NJ.

‡GE Healthcare, Buckinghamshire, UK.

§LightSpeed 4.X, LightSpeed 16, Technical Reference Manual, CE 0459, GE Healthcare, Buckinghamshire, UK.

this data sheet, to change the kV from 80 to 120, while keeping the $CTDI_{vol}$ constant, the mA needed to be decreased by a factor of 0.36. The next protocols were as follows: 120 kV, a pitch of 1.75, and 144 mA (400×0.36) and 120 kV, a pitch of 0.562, and 46 mA (128×0.36). This CT scanner only allowed mA settings in increments of 5 and therefore automatically changed the previous mA settings as follows: 128 to 130, 144 to 145, and 46 to 45.

A detector configuration of 16×0.625 mm and a beam collimation of 10 mm were used along with a "small" scan field of view. The image reconstruction parameters were a display field of view of 25 cm, a 1.25 mm slice thickness, a 0.625 mm slice reconstruction interval, and the "detail" algorithm. The protocols were repeated if severe motion artifact was detected by subjective evaluation during the scan. The original scanned images were manipulated on a separate workstation to obtain symmetric transverse plane images of the thorax. Subsequent multiplanar reformatting was performed to obtain dorsal and sagittal images, reconstructed with a 0.625 mm slice thickness and a 0.312 mm slice reconstruction interval.

The CT protocols were nonrandomized for the first 10 cats and randomized for the second 10 cats. The data from randomized and nonrandomized cats were evaluated for statistically significant differences.

For each protocol, total scan time and radiation dose measurements were recorded, the latter based on the scanner-generated $CTDI_{vol}$ values for a 16 cm phantom. The total time spent on CT was recorded for each cat from the time the cat entered the CT room until the time the cat left the CT room.

Quantitative image analysis was performed using a GE Advantage Workstation.‡ All measurements were performed on the original 1.25-mm-thick transverse images by one author (C.R.O.). Signal intensity of the pulmonary parenchyma (SI_{lung}) was defined as the attenuation (CT numbers in Hounsfield units [HU]) measured by placing a circular region of interest (ROI) in the dorsal pulmonary parenchyma at the level of the caudal thorax. The ROI size was 22 mm^2, the largest possible that could be drawn while avoiding the inclusion of bronchi and vessels.

Signal intensity of background (SI_{backgr}) was defined as the attenuation measured by placing a circular ROI in the paraspinal muscle at the level of the caudal thorax.[18] The ROI size was 45 mm^2, the largest possible that could be drawn while avoiding the inclusion of adjacent bones. To minimize bias from a single measurement for both SI_{lung} and SI_{backgr}, the measurements were made at five different locations in five subsequent images and the mean value was used for further calculations.

‡GE Healthcare, Buckinghamshire, UK.

Contrast was calculated as $SI_{lung} - SI_{backgr}$. The background noise was calculated on a phantom. The phantom was a round plastic container measuring 14.5 cm in diameter (approximately the diameter of the chest in a cat) and with a 2.0 mm wall thickness that was filled with water. ROIs of 400 cm^2 were placed in the center of the phantom in five subsequent images for each protocol. Averaged numbers were used for further calculations.

Signal-to-noise ratio (SNR) was calculated by dividing the mean CT number of the lung by the background noise (SI_{lung}/noise). Contrast-to-noise ratio (CNR) was calculated as follows: $CNR = (SI_{lung} - SI_{backgr})/\text{noise}$.[18]

The lateral and dorsoventral diameters of the thorax were measured for each cat at the level of the widest dimension of the thoracic cavity by placing the cursor on the edge of the skin. For cats aligned with the limbs in contact with the chest, the limbs were included in the measurements.

All images were initially evaluated qualitatively by one investigator (C.R.O.). The CT protocols were hidden from each image. During this first review, any artifacts encountered were recorded. These included blurred liver margins, helical–helical, motion, and windmill artifacts. Windmill artifact consists of black/white patterns that spin off of high contrast features that vary along the longitudinal (z-) axis. When the images are viewed in the cine mode, the artifact appears to spin like a windmill. In dorsal or sagittal images, they appear as bands.[19] The helical–helical artifact appeared as large areas in the lung with no attenuation. Helical–helical artifact, like windmill, is related to the need for data interpolation in helical scanning, which can result in areas of artificially high or low CT numbers near regions of large CT number changes.

For subsequent analysis, all data sets were evaluated by two board-certified radiologists and one certified CT technician. Images were randomized and displayed in transverse plane in the lung window (window level = −500, window width = 1500). Readings were performed independently for liver margins, windmill, and helical–helical artifact, and in consensus for motion artifact; evaluators were not aware of CT acquisition parameters for any image. A standardized questionnaire was used for image evaluation as follows: (1) liver margins: sharp—0, blurred—1; (2) helical–helical artifact: absent—0, present—1; (3) windmill artifact: absent—0, present—1; (4) motion artifact: absent—0, minimal—1, moderate—2, severe—3. Motion artifact was ranked according to the following locations: cranial thorax, if the motion artifact appeared predominantly cranial to the heart but not including the heart; middle thorax, if the motion appeared predominantly cranial to the liver but not including the liver; and caudal thorax, if the motion appeared predominantly from where the liver begins until the end of the thorax. Images were assigned the most severe score. The overall score for

motion artifact for each cat was considered to be the highest score among the locations. For each protocol, the percentage of slices affected by motion was calculated for each cat in which motion was found. Finally, for liver margins, helical–helical, and windmill artifacts, the number of times each score appeared combining all three evaluators was calculated and compared among protocols.

The Kolmogorov–Smirnov test was used to evaluate the distribution of the data. Normally distributed data were reported by mean, standard deviation (SD), and minimum–maximum values, while nonnormally distributed data were reported by median, 10–90%, and minimum–maximum values. A two-way ANOVA test was used to compare the protocols between the randomized vs. nonrandomized cats for SI (muscle and lung), noise, contrast, SNR, and CNR. For $ETCO_2$, FiO_2, temperature, and respiratory rate, nonnormally distributed data were analyzed using Friedman's test, while a repeated-measures general linear model was performed for normally distributed data. Post hoc tests were used to compare differences to time 0 when significant. A one-way ANOVA test was performed to compare the protocols for SI (muscle and lung), noise, contrast, SNR, and CNR data. A Pearson's Correlation regression analysis was used to compare the different outcomes (SI in muscle and lung, noise, contrast, SNR, and CNR) with the variables protocol, age, weight, width and height of thoracic cavity, and total time at CT.

Differences in the protocols between the evaluators were compared using the χ^2 test for homogeneity. When one box was less than 5, the Fisher exact test was used. For liver, helical, and windmill artifacts, κ statistic was used to assess the level of agreement between evaluators. A Fisher exact test was used to compare each protocol for liver, helical–helical, and windmill artifacts. A Kruskal–Wallis test was used for the comparison of protocols for overall motion and to compare motion among the three different locations in the chest. Because a difference was found for overall motion among the protocols, a Mann–Whitney test was used to compare each protocol. A $P<0.05$ was considered to be statistically significant. Statistical analyses were performed using two commercial software programs.¶,‖

Results

Phase 1

The final design of the VetMousetrap™ was a transparent acrylic tube with a wall thickness of 5 mm, outer diameter of 21 cm, and length of 40 cm (Fig. 1). The tube was cut lengthwise during construction, resulting in top and base portions. The base portion has supportive legs with rounded edges. The construction has no moving parts or hinges and has a secure closure without additional metallic or plastic components. The closure is affected by intimate interlocking upper and base components. The sides are not sealed, which allows excess gas to escape, and prevents pressure, heat, and humidity accumulation. The cats can be monitored visually throughout the imaging procedure and removed quickly in case of an emergency. Oxygen and catheter line access is simple. Catheter line access is via a slot in the base, which, after closure with placement of the top component, results in an oblong small 6×6 mm hole. The device has low attenuation (approximately 54 HU) and did not cause visible artifacts during CT image acquisition.

FIG. 1. The VetMousetrap™. Ports for catheter access (thin arrows) and oxygen administration (thick arrows) are present on both ends of the device. The device is transparent, portable, easy to clean, narrow, has no metal components, and has a symmetric design.

$ETCO_2$, FiO_2, temperature inside the device, and respiratory rates of the cats are presented in Tables 1 and 2. During the measurements, one cat was active after being placed in the device and kept moving during the 30-min interval. The other nine cats remained quiet most of the time, with no overt signs of stress.

There was a statistically significant difference in $ETCO_2$ levels at time 0 compared with times 5–30 min; however, there was no difference in $ETCO_2$ levels over time after 5 min. The maximum CO_2 level inside the device at all

TABLE 1. CO_2 and FiO_2 Measurements Inside the VetMousetrap™

	CO_2 (mmHg)			FiO_2 (%)		
Time (min)	Mean	SD	Min–Max	Mean	SD	Min–Max
0	0*	0–5†	0–6	20.7*	20–30†	20–33
5	10.5	4.1	6–19	53.2	17.1	30–85
10	10.1	4.1	3–16	64.2	14.2	44–85
15	11.1	3.9	7–17	66.8	17.7	36–93
20	11.5	4.9	3–17	61.1	20.4	32–95
25	9.2	4.1	5–18	68.1	19.5	40–95
30	9.7	4	4–18	65.9	15.6	42–86

*Median. †80% Percentile. CO_2, carbon dioxide, measured as end-tidal carbon dioxide; FiO_2, fraction of inspired oxygen, FiO_2 at room air = 21%; SD, standard deviation; Min–Max, minimum–maximum.

¶MedCalc Software, Mariakerke, Belgium.
‖SPSS, IBM Company, Chicago, IL.

TABLE 2. Temperature Inside the VetMousetrap™ and Respiratory Rate of Cats

	Temperature (°C)			RR (bpm)*		
Time (min)	Mean	SD	Min–Max	Mean	SD	Min–Max
0	23.5	0.9	22–24	52.9	14.8	24–72
5	25.4	1.5	23–27	51.3	13.8	30–66
10	25.9	1.2	24–28	47.6	14.3	28–66
15	26.1	1.1	25–28	50.7	18.5	28–80
20	26.4	1	25–29	47.3	15.8	28–66
25	26.7	1	25–29	47.3	14.6	28–66
30	26.8	1	26–29	46.9	14.7	28–68

*RR, respiratory rate in breaths per minute. Recorded in nine cats. SD, standard deviation; Min–Max, minimum–maximum.

times was 19 mmHg. There was a significant difference in FiO_2 levels at time 0 compared with times 5–30 min, with the levels increasing over time.

There was a significant difference in FiO_2 levels comparing measurements at 5 min with those at 10, 15, and 25 min. No difference was found in comparing measurements at 5 min with those at 20 or 30 min.

Similarly, a significant difference in temperature was found at time 0 compared with times 5–30 min, with the temperature increasing over time. The highest measurement, of 29°C, was found at 20, 25, and 30 min. Respiratory rate was recorded in nine of the 10 cats, and no difference was found over time. The mean respiratory rate at time 0 was 53 breaths per minute (bpm), while at time 30 min, it was 47 bpm.

Phase 2

Demographic and morphologic parameters of the cats are shown in Table 3. The mean age of the cats was 7.5 years and the mean body weight was 4.5 kg. There was no statistical significant difference between randomized and nonrandomized cats, and the statistical analysis was performed adding these two groups. The mean total time at CT was 12.5 min, with a range of 5–28 min. With the exception of five cats, the total time at CT was below 15 min.

The CT protocols are displayed in Table 4. In 20 out of 22 cats, CT was completed without complications. Two cats showed signs of overt stress and attempted to escape from the VetMousetrap™. The first attempt to image one of these cats resulted in extreme motion artifact; the CT examination was terminated. The second cat remained in dorsal recumbency and was pushing the top of the device with all four limbs and CT examination was not attempted. These two cats were excluded from the study. The remaining 20 cats showed no signs of physical or respiratory distress and remained in a sternal resting position for almost the entire CT examination. Some cats moved their head from side to side and some would flip 180° inside the device and then remain still. Approximately 50% of cats had at least one protocol repeated due to motion artifact. The images were acquired from cranial to caudal in most cats. Most original transverse plane images were characterized by mild to moderate obliquity before on-line manipulation. Presumed pulmonary atelectasis was present in one cat and seen in all protocols for this cat. This appeared as a small region of patchy alveolar pattern in a dependent region of the lung.

TABLE 3. Data Distribution of Phase 2 Cats

	Mean	SD	95% CI	Min–Max
Age (years)	7.5	4.5	5.4–9.7	1–15
BW (kg)	4.6	1	4.2–5.1	3–6.1
WC (cm)	12.8	2.7	11.6–14	8.4–17.5
HC (cm)	14.3	1.4	13.7–15	11.9–16.5
Total time at CT (min)	12.7	6	9.9–15.6	5–28

BW, body weight; WC, width of chest; HC, height of chest; SD, standard deviation; CI, confidence interval; Min–Max, minimum–maximum.

TABLE 4. Computed Tomography (CT) Protocols

	Protocol 1	Protocol 2	Protocol 3	Protocol 4
Tube voltage (kV)	80	80	120	120
Pitch	0.562	1.75	0.562	1.75
Tube current (mA)	130	400	45	145
mA	65	200	22.5	72.5
Effective mAs	116	114	40	41
Rotation time (s)	0.5	0.5	0.5	0.5
Field of view (cm)	25	25	25	25
Slice thickness (mm)	1.25	1.25	1.25	1.25
Increment (mm)	0.625	0.625	0.625	0.625
Total scan time (s)	36.7	11.9	36.7	11.9
$CTDI_{vol}$ (mGy)	8.71	9.39	8.36	8.66

$CTDI_{vol}$, volume CT dose index.

The results for the quantitative evaluation are presented in Table 5. A statistically significant difference was found for SNR and CNR among all protocols. Among the same kV, protocols with a higher pitch had the highest SNR and CNR and among the same pitch, protocols with a higher kV had the highest SNR and CNR. The contrast was higher in protocols with lower kV although the difference

TABLE 5. Quantitative Results

	Protocol 1		Protocol 2		Protocol 3		Protocol 4	
	Mean	SD	Mean	SD	Mean	SD	Mean	SD
SI_{lung}	-827.8^{a}	53.5	-831.2^{a}	59.2	-814.3^{a}	56.2	-822.6^{a}	59
SI_{backgr}	61.9^{a}	3.2	62.4^{a}	4.9	60.4^{ab}	2.5	58.7^{b}	5.4
Contrast	765.9^{a}	53.2	768.8^{a}	58.5	753.9^{a}	57.4	763.9^{a}	61.4
Noise	20.4	0.09	17.8	0.2	18.5	0.2	16.3	0.1
SNR	40.5^{a}	2.6	46.7^{b}	3.2	44^{c}	3	50.6^{d}	3.5
CNR	37.5^{a}	2.6	43.2^{b}	3.3	40.7^{c}	3.1	47^{d}	3.8

Within a row, protocols with different letters show statistically significant difference. SI_{lung}, signal intensity in the lung; SI_{backgr}, signal intensity in the background; SNR, signal-to-noise ratio; CNR, contrast-to-noise ratio.

TABLE 6. Pearson's Correlation Coefficient of Quantitative Variables

	SI_{lung}	SI_{backgr}	Noise	SNR	CNR
Protocols	0.06*	−0.3	−0.5	0.4	0.3
Age (years)	−0.4	−0.25*	−0.22*	0.3	0.3
BW (kg)	0.37*	0.5	0.3	−0.43*	−0.4
WC (cm)	0.4	0.07*	0.3	−0.4	−0.4
HC (cm)	−0.14*	0.16*	−0.01*	0.06*	0.06*

*Not statistically significant. SI_{lung}, signal intensity in the lung; SI_{backgr}, signal intensity in the background; SNR, signal-to-noise ratio; CNR, contrast-to-noise ratio.

was not statistically significant. There was no statistically significant difference for SI_{lung} among protocols. The results for noise and $CTDI_{vol}$ were similar for all four protocols (Tables 4 and 5). Results of regression analysis are summarized in Table 6. There was a statistically significant, although weak, positive correlation of body weight with SI_{backg} and noise, and negative correlation with CNR. Similarly, width of the thorax had a weak positive correlation with SI_{lung} and noise, and a negative correlation with CNR and SNR. Age had a significant, although weak positive correlation with SNR and CNR, and a negative correlation with SI_{lung}. Height of the thorax was not correlated with any of the parameters.

Qualitative results are summarized in Tables 7–9. The interobserver agreement was moderate to substantial for the evaluation of liver margins, substantial for helical–helical artifact, and substantial to almost perfect for windmill artifacts.[20] For overall motion, protocols with high pitch had significantly less motion artifact compared with protocols using low pitch. For location of motion artifact, there was no statistical difference based on the reader's score for any protocol in any location. Overall, 75 out of 80 (94%) examinations were judged to have no or minimal motion artifact.

There was a statistically significant difference for windmill and helical–helical artifacts between protocols with 1.75 and 0.562 pitch, with 0.562 pitch protocols having less windmill and helical–helical artifacts (Figs. 2–5). There was also a significant difference in liver margins between protocols with different pitches, with higher pitches showing sharper liver margins than lower pitches (Fig. 6A–D).

TABLE 7. κ Statistic Interobserver Agreement

Evaluator*	Liver Margins	Helical Artifact	Windmill Artifact
A–B	0.59	0.72	0.90
A–C	0.70	0.72	0.75
B–C	0.72	0.74	0.80

*Evaluator A and C: board-certified radiologists; evaluator B: certified CT technician. <0 less than chance agreement; 0.01–0.20 slight agreement; 0.21–0.40 fair agreement; 0.41–0.60 moderate agreement; 0.61–0.80 substantial agreement; 0.81–0.99 almost perfect agreement.

TABLE 8. Percentage of Slices Affected by Motion Artifact

Protocol	1	2	3	4
Cats				
1	3% (8/241)	0%	9% (23/243)	0%
6	10% (25/243)	0%	15% (35/230)	0%
8	10% (17/174)	0%	0%	0%
9	7% (15/216)	0%	0%	0%
10	7% (16/229)	0%	6% (13/233)	0%
11	0%	0%	9% (21/243)	0%
12	0%	0%	10% (21/206)	0%
13	9% (19/207)	0%	8% (16/198)	0%
14	0%	0%	8% (17/202)	0%
15	0%	4% (6/162)	0%	0%
16	6% (11/185)	0%	4% (7/175)	0%
17	6% (11/198)	19% (37/199)	0%	7% (14/198)
20	0%	0%	9% (18/192)	0%

Cats 2, 3, 4, 5, 7, 18, and 19 had no images affected by motion.

Discussion

Our goals were to describe the design of a new low attenuating transparent device that also functions as a clinically supportive environment and to compare protocols for CT of the thorax in awake cats inside the device. The VetMousetrap™ allowed cats to be imaged without direct manipulation, and CT examination was deemed less stressful than thoracic radiographs because there was minimal stress of restraint and no stress of positioning. CT examinations were successfully performed in 20 of 22 cats when placed inside the VetMousetrap™. The remaining cats tolerated the device very well and remained still for almost the entire CT examination.

Based on physiologic measurements, the VetMousetrap™ was safe and well tolerated by the cats. The difference in $ETCO_2$ levels at time 0 compared with times 5–30 min was expected because initially no cat was inside the device, and therefore, the levels of $ETCO_2$ for all but one cat were 0 mmHg. There was no statistically significant difference in $ETCO_2$ levels over time after 5 min, indicating that the levels of CO_2 inside the device do not increase for up to a period of 30 min. Although not statistically significant, decreasing CO_2 levels were found at the maximum times (25 and 30 min) compared with initial times. The maximum CO_2 level inside the device at any time was 19 mmHg.

TABLE 9. Number of Times Each Score Appeared Combining All Three Evaluators

	Liver Margins				Helical Artifact				Windmill Artifact			
Protocol	1	2	3	4	1	2	3	4	1	2	3	4
Score												
0	5^a	49^b	4^a	53^b	47^a	2^b	50^a	3^b	57^a	1^b	53^a	3^b
1	55^a	11^b	56^a	7^b	13^a	58^b	10^a	57^b	3^a	59^b	7^a	57^b

Within a row, protocols with different letters show statistically significant difference. Liver margins: sharp—0, blurred—1; helical artifact: absent—0, present—1; windmill artifact: absent—0, present—1.

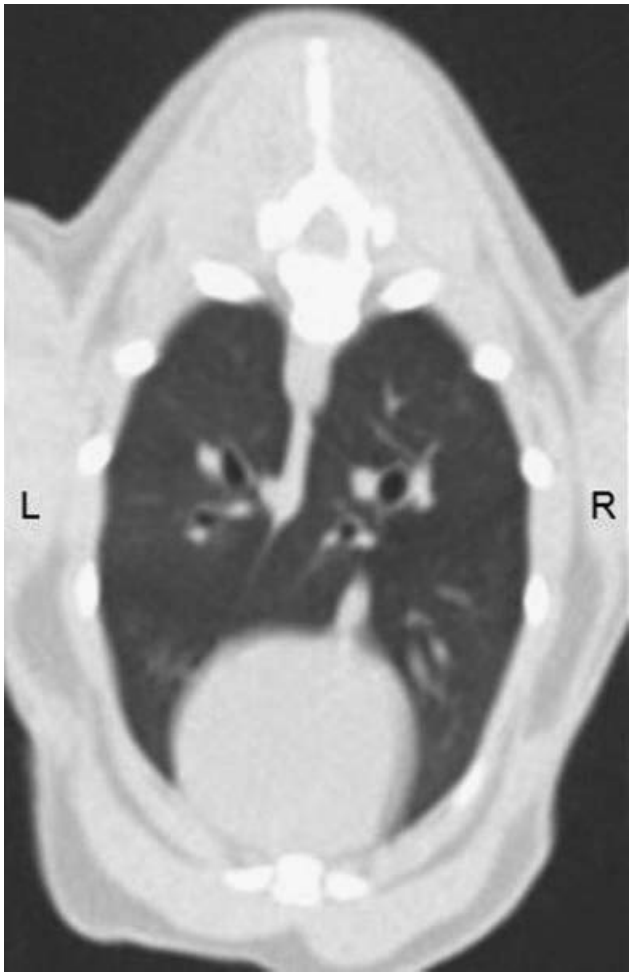

Fig. 2. Transverse computed tomographic (CT) image of the caudal thorax of cat 7 using protocol 1 (80 kV, 0.562 pitch). No windmill or helical–helical artifacts were detected. Window width = 1600, window level = −600.

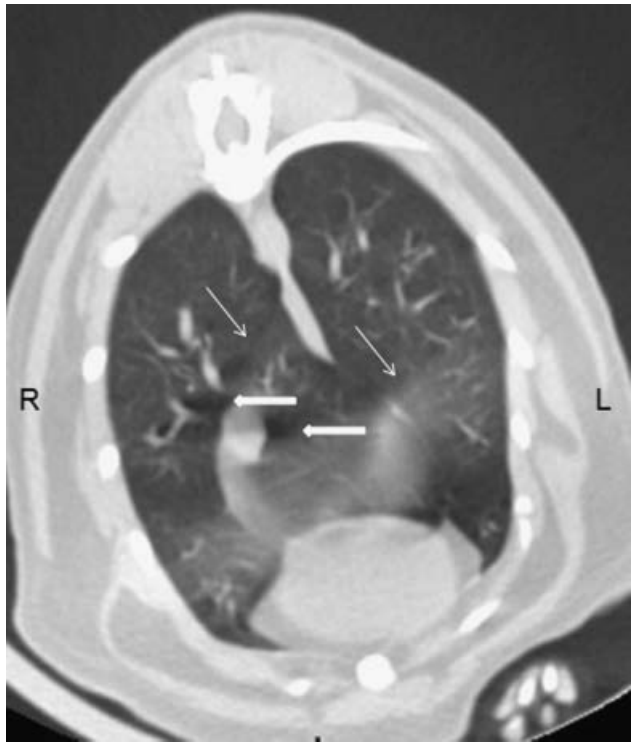

Fig. 3. Transverse computed tomographic (CT) image of the caudal thorax of cat 10 using protocol 2 (80 kV, 1.75 pitch). The vanes of the windmill artifact are visible (thin arrows). The helical–helical artifact is also visible (thick arrows). Window width = 1600, window level = −600.

The significant difference in FiO_2 levels found at time 0 compared with times 5–30 min with increasing levels of oxygen up to 25 min indicates that the device worked properly as an oxygen provider. An oxygen flow rate of 2 l/min provided a mean FiO_2 inside the device of 53% at 5 min and 68% at 25 min with a maximum of 95% FiO_2 (FiO_2 at room air = 21%).[21,22]

There was a significant difference in temperature levels inside the device over time, with the highest mean of 26.8°C at 30 min. Overall, the mean temperature was within a narrow and safe range of 23.5–26.8°C. There was no significant change in the respiratory rate of the cats, indicating that the temperature and CO_2 rise were not significant to cause any increase in respiratory rate and effort. This is most important for cats in respiratory distress as the device should not contribute to increased respiratory rate or effort.

Respiratory rate was recorded in nine of 10 cats and no statistically significant difference was found over time. The mean respiratory rate at time 0 was 53 bpm and at time 30 min, it was 47 bpm. These values are mildly above the normal (20–44 bpm), possibly indicating some degree of stress.[23] However, the fact that they were higher at 0 min than at any other time could indicate that the cats were stressed by other reasons such as being in the hospital and being handled, rather than by the device itself. After 20 min inside the device, the respiratory rates began to decrease and achieved the lowest mean at the maximum time (30 min).

The CT protocols used in this study were adapted from human pediatric CT. When performing CT imaging of awake cats, two similarities can be found with human pediatric CT: the need to depict very small anatomic structures, such as peripheral bronchi, and the fact that both awake cats and children can often be uncooperative patients producing motion artifact. To address these two problems, we compared protocols with a low and high kV to test for differences in image contrast and with a low and high pitch to test for differences in image artifacts.

In humans, a reduction in kV is associated with an increase in image contrast. Changes in kV alter both the quality and the quantity of photons. By changing the tube voltage, the number of photons produced changes and the photons have a different energy.[16] In this study,

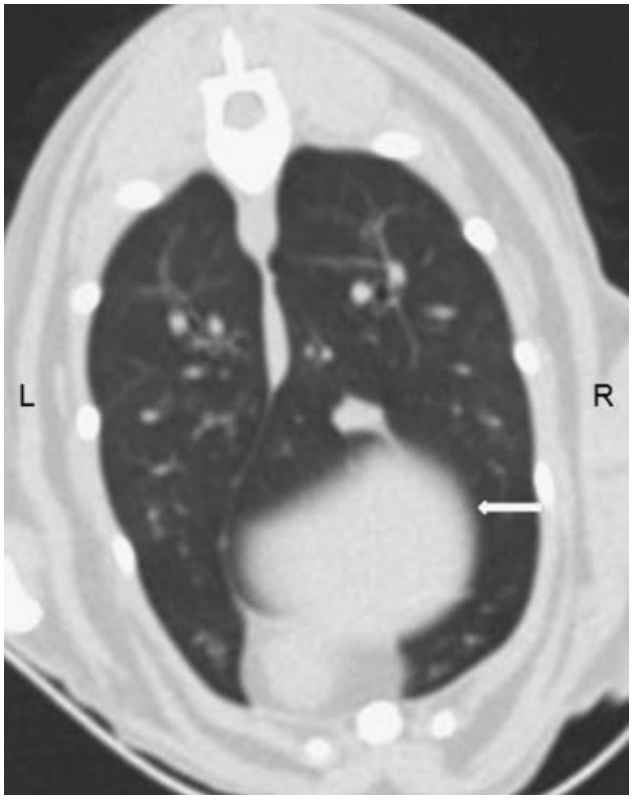

FIG. 4. Transverse computed tomographic (CT) image of the caudal thorax of cat 1 using protocol 3 (120 kV, 0.562 pitch). No windmill or helical–helical artifacts were detected. There is mild blurring of the liver margin (arrow). Window width = 1600, window level = −600.

FIG. 5. Transverse computed tomographic (CT) image of the caudal thorax of cat 5 using protocol 4 (120 kV, 1.75 pitch). Multiple regions of helical–helical artifact are visible (arrows). Window width = 1600, window level = −600.

protocols with a lower kV showed a better contrast, although not statistically significant, but slightly lower SNR and CNR compared with protocols with higher kV. The higher SNR can be explained by the increased tube voltage on 120 kV, but the higher CNR in protocols with higher kV was not expected. An important consideration is the fact that the contrast measurements were performed between soft tissue and air in the lung. This contrast is not strongly dependent on kV because by definition, the CT contrast scale has a difference of 1000 HU between air and water at all kV settings. In looking at contrast or CNR between soft tissues or bone, one would expect an increase or improvement at lower kV. Also, in situations where contrast media are used, the image contrast and CNR will be increased substantially at lower kV. It is well documented in humans that besides increases in soft-tissue contrast, low kV CT protocols enhance the iodine-induced contrast, and thus reduces the amount of iodinated contrast media required to image lower weight patients, because the attenuation of iodine-based contrast media increases with reduced X-ray energy.[24–26] Although statistically significant, the difference in SNR and CNR related to kV in this study was very small and probably not clinically relevant. The impact of this difference on the subjective evaluation of image quality was not assessed. The higher SNR, CNR, and slightly lower noise in the protocols with 1.75 pitch can be explained by the fact that increasing pitch causes widening of the slice sensitivity profile, a measure of the ability of the CT scanner to precisely limit the information that makes up the image to a defined slice of tissue. If the individual detector collimation does not change, images acquired with higher pitch are effectively thicker slices.[16,27] The slice thickness has a strong influence on the number of photons used to produce the image. Thicker slices use more photons and have a better SNR.[28] This means that the apparent advantage of higher pitch in SNR and CNR is artificial and only obtained through a decrease in the longitudinal resolution.

Patient motion can cause significant artifacts, which usually appear as shading or streaking in the reconstructed image.[29] Motion is decreased with shorter imaging time in two ways. First, the amount of motion during each single slice acquisition decreases. Second, the ability of the patient to cooperate is improved with a shorter overall duration of the scan, at least in humans. Scan time can be decreased using a faster gantry rotation.[16] The scan time also affects the longitudinal (z-axis) coverage. The longitudinal cover-

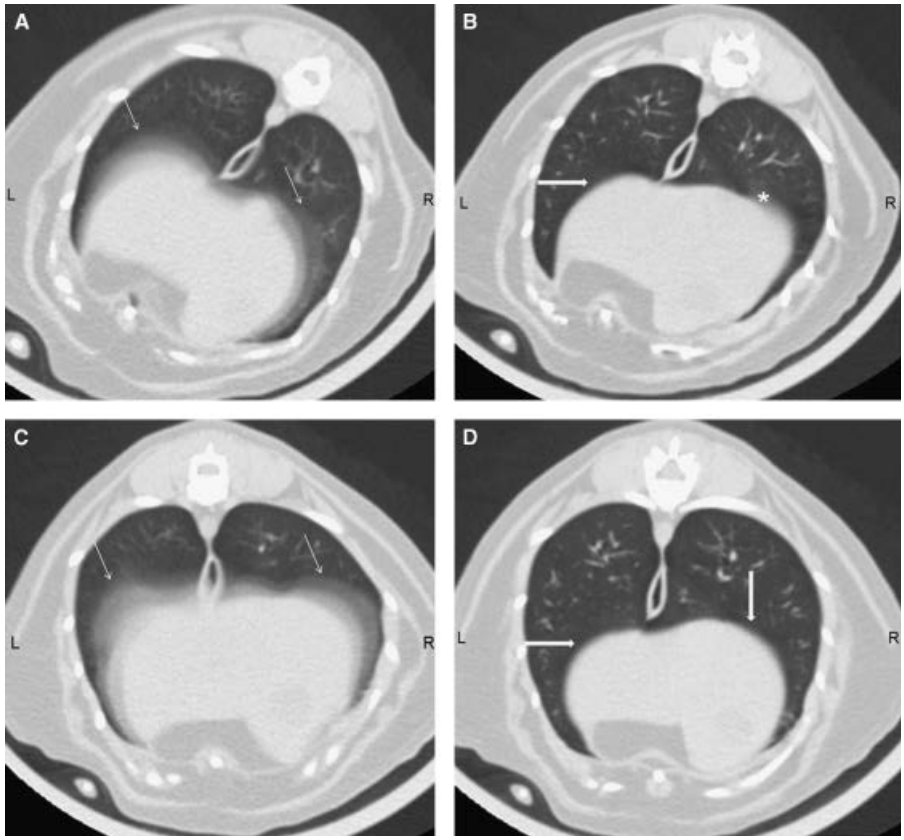

Fig. 6. Transverse computed tomographic (CT) images of the caudal thorax of cat 11: (A) Protocol 1, 80 kV, 0.562 pitch. (B) Protocol 2, 80 kV, 1.75 pitch. (C) Protocol 3, 120 kV, 0.562 pitch. (D) Protocol 4, 120 kV, 1.75 pitch. Liver margins are blurred in protocols 1 and 3 (thin arrows). Liver margins in protocols 2 and 4 are sharp (thick arrows). In (B), a vane from the windmill artifact is visible (asterisk). Window width = 1600, window level = −600.

age can be calculated by multiplying the longitudinal beam collimation, pitch, and scan time, and by dividing by the gantry rotation time.[30]

The selection of pitch is a trade-off between patient coverage and accuracy. Larger pitches reduce scanning time, allowing more coverage of a patient per unit of time, but slice data must be interpolated using scan data that is farther from the actual slice, producing more artifacts.[31,32] In pediatric thoracic CT, although no single helical CT technique has gained universal acceptance, in general, a pitch of at least 1.3 is used and several authors use a pitch from 1.3 to 1.6.[16] When evaluating CT protocols for pulmonary nodule detection in dogs, pitches of 1.5 and 2 were tested and both yielded good image quality.[32] In evaluation of CT protocols for the cervical and lumbar spine of dogs, increasing pitch from 0 to 2 was associated with significantly poorer scores for half of the examined categories.[33]

To minimize motion artifact, we used the fastest available rotation time (0.5 s) and tested protocols with a higher pitch. We hypothesized that images acquired with 1.75 pitch would result in less motion artifact, supported by the results of all evaluators. Most CT examinations judged to have moderate or severe motion artifact were obtained with protocols using 0.562 pitch. This difference was expected as the scan time using 1.75 pitch was approximately 30% of the scan time using 0.562 pitch. However, even though a statistically significant difference was found between high and low pitch for motion artifact, overall, motion artifact was considered to be absent or minimal for the majority of examinations regardless of protocol, and moderate or severe motion was present in a very small percentage of examinations (Table 8). Furthermore, all images were considered to be of excellent diagnostic quality, even those ranked as having moderate or severe motion. Finally, all CT examinations were ranked by the worse score present, regardless of the number of slices affected. In this regard, only 5% (4/80) of the examinations had motion artifact present in more than 10% of the total number of slices.

Liver margins were considered to be consistently blurred on the low-pitch protocols, but the degree of blurring was very mild and did not appear to affect the overall image quality.

Although protocols with a higher pitch showed less motion artifact, substantial helical and windmill CT artifacts were found using these protocols with a moderate to good

interobserver agreement. Helical and windmill artifacts were significant in most images with 1.75 pitch and these artifacts were almost absent in the images acquired with 0.562 pitch.

It is a common understanding that the windmill artifact is due to the need for data interpolation in helical scanning. Generally, the amplitude of the windmill artifact decreases as the number of detector rows increases: the windmill artifact in 64-slice CT is less than that in 16-slice CT.[34] Both windmill and helical–helical artifacts gradually increase as pitch is increased.[35]As helical pitch increases, the number of detector rows intersecting the image plane per rotation increases and the number of "vanes" in the windmill artifact increases, but the strength of the artifact in each vane decreases proportionately.[29] The most recommended practice to avoid this artifact is to scan using the thinnest possible individual detector collimation, in other words, fine longitudinal sampling, and reconstructing thick images, such as 1 and 2 mm or thicker images. For example, a detector collimation of 16×0.625 mm is preferable to 16×1.25 mm or 8×2.5 mm. Obtaining thicker images than the individual detector collimation is equivalent to longitudinal filtering, which means a substantial compromise on the longitudinal resolution, but also a decrease in image noise.[36]

Near-isotropic images could be acquired by reformatting the 0.625 mm slice thickness images in dorsal and sagittal planes. Recent advances in multidetector CT technology have made the acquisition of isotropic data feasible with use of a narrow configuration of the detector array so that only the smallest detector elements are exposed.[37] Through several generations of CT scanners, long-axis resolution was consistently inferior to short-axis, or transverse, spatial resolution. Spatial resolution in the transverse plane is limited by pixel size. Within a matrix of 512×512 and a scanning field of view of 25 cm, the pixels that constitute each axial image are squares with a length of approximately 0.49 mm on each side. Using the "detail" reconstruction algorithm, the spatial resolution due to the algorithm is about 0.6 mm. Thus, a slice thickness in the range of 0.5–0.8 mm is required to achieve similar spatial resolution in all three dimensions. If the thickness of the axial slice is taken into account, the square pixels are converted to 3D voxels. When data are reconstructed to achieve similar dimensions in all three planes, it consists of cube-shaped voxels and the images are considered to be isotropic. Isotropic imaging minimizes the importance of patient positioning and obviates the need to obtain transverse, dorsal, and sagittal planes directly because reformation in any desired plane will have a spatial resolution similar to that of the original plane.[15,30,35,37,38] This is especially important when imaging awake cats, as the original images are acquired in a nontraditional oblique plane depending on the position of the cat inside the device.

We hypothesized that the images would have no lung lobe atelectasis as the cats were scanned without sedation or general anesthesia, and this was confirmed in all but one cat, in which atelectasis occurred probably as a result of recumbency.

When developing the protocols, we used information from the technical data sheet of the CT scanner‡ to adjust the scan parameter to provide the same $CTDI_{vol}$ for each of the four protocols used. When performing the scans, we recorded the $CTDI_{vol}$ generated by the CT scanner and the displayed results were, in fact, similar for all four protocols. The CTDI is the dose measured in a 16 or 32 cm acrylic phantom (the CTDI phantom), while the $CTDI_{vol}$ is a weighted average of surface and central dose measurements in the phantom so as to approximate the average dose to the phantom volume when the effect of pitch on dose is also taken into account. The $CTDI_{vol}$ is widely used in human adult and pediatric CT to evaluate different protocols on a single CT scanner because an initial comparison of different techniques can be performed easily. Improvements in image quality for a consistent dose as well as decreases in dose while maintaining acceptable image quality can be suggested, and then evaluated in regular use.[16] When choosing protocols for CT in humans, there is always a trade-off between image quality and dosage. Radiologists and technicians must balance protocol selection between resolution, noise, and contrast to achieve good image quality and keep patient exposure as low as reasonably achievable.[39] In veterinary medicine, radiation exposure is not as much of a concern as it is in humans; however, studies evaluating radiation dose and safety associated with routine imaging diagnosis are lacking. We decided to choose protocols with a relatively low and constant dose as the cats would be subjected to multiple scans.

In pediatric CT, there is a recommendation for using a sharper algorithm for the reconstruction of lung images.[16] Sharper algorithms delineate object margins more clearly at the expense of increased image noise. Less sharp algorithms reduce noise, allowing a larger low-contrast object to become more visible, although edges will be blurrier and fine detail lost. A moderately sharp (detail) algorithm was used in this study, which is somewhat sharper than smooth or standard algorithms, but less sharp compared with "bone" algorithms. This algorithm was chosen to yield the best compromise between resolution and image noise.[31]

Although positive, the correlation found between body weight and noise, and width of the chest and noise was very weak and probably not clinically relevant. This correlation could be explained by the fact that cats in this study had a wide range of body weights and thoracic cavity widths, and this could increase image noise if tube current and voltage are not changed. If the noise increases, and contrast and

‡GE Healthcare, Buckinghamshire, UK.

signal intensity do not increase proportionally, it is expected that CNR and SNR will vary in the opposite direction.

The mean total time in the CT scanner in this study was similar to the time required to perform a three-view thoracic study in our institution in a cooperative cat with experienced holders, which is on average 10 min. However, in a clinical situation when only one protocol would be used, the total time in the CT scanner when scanning awake cats would be reduced significantly. Furthermore, CT examinations were believed to be less stressful for the cats, as no direct manipulation was necessary, and safer for personnel due to the absence of radiation exposure.

The measurements of FiO_2 inside the VetMousetrap™ could have been affected by the fact that some cats turned around constantly, resulting in temporary blocking of the flow of oxygen. Although motion artifact was almost absent, some cats were scanned multiple times when the images were initially considered nondiagnostic. When dealing with an uncooperative patient, the advantages of performing CT without general anesthesia, such as: the possibility to scan a patient that otherwise would not be subjected to CT due to clinical instability, the absence of lung atelectasis, and faster and less expensive examinations, could be considered to be a trade-off with the potential radiation hazard and increased tube usage that could result from multiple scans.

During the CT scan, the ROIs were not at the isocenter of the CT machine because prescan scouts were not made and it was not possible to know where the cat would be positioned inside the VetMousetrap™. This could have been responsible, at least in part, for some image degradation. When testing pitch, we decided to use two extreme values, and 0.938 and 1.375 pitches, not tested in this study, could potentially result in a better balance between helical and motion artifacts. It would also have been of interest to assess whether a qualitative difference can be detected between the two different kV; however, this was not done in this study. Finally, the protocols evaluated here can vary significantly with different CT machines and should only be used as a guideline.

In conclusion, the VetMousetrap™ is a device that provides effective oxygen and catheter-based therapy while keeping safe temperature and CO_2 levels, and allows CT imaging of nonsedated, unanesthetized cats. Coupled with a 16-slice CT scanner, the device allowed whole-body images to be acquired successfully in a very short period of time with excellent spatial resolution in all three planes and negligible motion artifact. Presumed lung lobe atelectasis was present in only one cat and deemed to be very mild. Protocols with 1.75 pitch had significant windmill and helical–helical artifact, which compromised image quality and therefore are not recommended. With 0.562 pitch, windmill and helical artifacts were almost absent and motion, although statistically higher compared with 1.75 pitch, was overall minimal and not considered to be clinically relevant. Based on these results and on the literature, we recommend a protocol of 80 kV, 130 mA, 0.5 s, and 0.562 pitch, with a 1.25 mm slice thickness and a 0.625 mm slice reconstruction interval for helical thoracic CT examination of awake cats using the VetMousetrap™. Protocol adjustments for cats with different body weights and conformations do not appear to be necessary. Future studies are needed that would evaluate the full range of available pitches and assess the subjective difference in image quality between 80 and 120 kV. The VetMousetrap™ has the potential to make a significant impact on the safety of the diagnostic imaging and case management of cats with respiratory compromise.

REFERENCES

1. White CS, Kuo D. Chest pain in the emergency department: role of multidetector CT. Radiology 2007;245:672–681.
2. Novelline RA, Rhea JT, Rao PM, Stuk JL. Helical CT in emergency radiology. Radiology 1999;213:321–339.
3. Cipone M, Diana A, Gandini G, Fava D, Trenti F. Use of computed tomography in thoracic diseases of small animals. Vet Res Commun 2003;27:381–384.
4. Henninger W. Use of computed tomography in the diseased feline thorax. J Small Anim Pract 2003;44:56–64.
5. Prather AB, Berry CR, Thrall DE. Use of radiography in combination with computed tomography for the assessment of noncardiac thoracic disease in the dog and cat. Vet Radiol Ultrasound 2005;46:114–121.
6. Burk RL. Computed tomography of thoracic diseases in dogs. J Am Vet Med Assoc 1991;199:617–621.
7. Yoon J, Feeney DA, Cronk DE, Anderson KL, Ziegler LE. Computed tomographic evaluation of canine and feline mediastinal masses in 14 patients. Vet Radiol Ultrasound 2004;45:542–546.
8. Johnson VS, Ramsay IK, Thompson H, Cave TA, et al. Thoracic high-resolution computed tomography in the diagnosis of metastatic carcinoma. J Small Anim Pract 2004;45:134–143.
9. Eisenkraft JB. Effects of anaesthetics on the pulmonary circulation. Brit J Anaesth 1990;65:63–78.
10. Staffieri F, Franchini D, Carella GL, et al. Computed tomographic analysis of the effects of two inspired oxygen concentrations on pulmonary aeration in anesthetized and mechanically ventilated dogs. AmJ Vet Res 2007;68:925–931.
11. Hedenstierna G, Rothen H. Atelectasis formation during anesthesia: causes and measures to prevent it. J Clin Monit Comput 2000;16:329–335.
12. Johnston C, Carvalho WBD. Atelectasias em pediatria: mecanismos, diagnóstico e tratamento. Rev Assoc Méd Bras 2008;54:455–460.
13. Nemanic S, London CA, Wisner ER. Comparison of thoracic radiographs and single breath-hold helical CT for detection of pulmonary nodules in dogs with metastatic neoplasia. J Vet Intern Med 2006;20:508–515.
14. Morandi F, Mattoon JS, Lakritz J, Turk JR, Wisner ER. Correlation of helical and incremental high-resolution thin-section computed tomographic imaging with histomorphometric quantitative evaluation of lungs in dogs. Am J Vet Res 2003;64:935–944.
15. Rydberg J, Sandrasegaran K, Ying J, Akisik F, Choplin RH, Tarver RD. Isotropic chest CT examination: diagnostic quality of reformats. Clin Radiol 2006;61:588–592.

16. Brody ASMD. Thoracic CT technique in children. J Thor Imag 2001;16:259–268.

17. Frush DP, Donnelly LF. Helical CT in children: technical considerations and body applications. Radiology 1998;209:37–48.

18. Szucs-Farkas Z, Kurmann L, Strautz T, Patak MA, Vock P, Schindera ST. Patient exposure and image quality of low-dose pulmonary computed tomography angiography: comparison of 100- and 80-kVp protocols. Invest Radiol 2008;43:871–876.

19. Silver MD, Taguchi K, Hein IA, Chiang B, Kazama M, Mori I. *Windmill artifact in multislice helical CT*. Paper presented at Medical Imaging 2003: Image Processing, 2003; San Diego, CA, USA.

20. Viera AJ, Garrett JM. Understanding interobserver agreement: the kappa statistic. Fam Med 2005;37:360–363.

21. Mann FA, Wagner-Mann CC, Branson KR. Transcutaneous oxygen and carbon dioxide monitoring in normal cats. J Vet Emerg Crit Care 1997;7:99–109.

22. Berent AC, Todd J, Sergeeff J, Powell LL. Carbon monoxide toxicity: a case series. J Vet Emerg Crit Care 2005;15:128–135.

23. Sigrist NE, Doherr MG, Spreng DE. Clinical findings and diagnostic value of post-traumatic thoracic radiographs in dogs and cats with blunt trauma. J Vet Emerg Crit Care 2004;14:259–268.

24. Sigal-Cinqualbre AB, Hennequin R, Abada HT, Chen X, Paul JF. Low-kilovoltage multi-detector row chest CT in adults: feasibility and effect on image quality and iodine dose. Radiology 2004;231:169–174.

25. Kalva SP, Sahani DV, Hahn PF, Saini S. Using the K-edge to improve contrast conspicuity and to lower radiation dose with a 16-MDCT: a phantom and human study. J Comp Assist Tomogr 2006;30:391–397.

26. Heyer CM, Mohr PS, Lemburg SP, Peters SA, Nicolas V. Image quality and radiation exposure at pulmonary CT angiography with 100- or 120-kVp protocol: prospective randomized study. Radiology 2007;245:577–583.

27. Polacin A, Kalender WA, Marchal G. Evaluation of section sensitivity profiles and image noise in spiral CT. Radiology 1992;185:29–35.

28. Bushberg JT, Seibert JA, Leidholdt EM, Boone JM (eds): The essential physics of medical imaging, 2nd edn. Philadelphia: Lippincott Williams and Wilkins, 2001.

29. Barrett JF, Keat N. Artifacts in CT: recognition and avoidance. Radiographics 2004;24:1679–1691.

30. Rydberg J, Liang Y, Teague SD. Fundamentals of multichannel CT. Radiol Clin North Am 2003;41:465–474.

31. Goldman LW. Principles of CT and CT technology. J Nucl Med Technol 2007;35:115–128.

32. Joly H, D'anjou M-A, Alexander K, Beauchamp G. Comparison of single-slice computed tomography protocols for detection of pulmonary nodules in dogs. Vet Radiol Ultrasound 2009;50:279–284.

33. Drees R, Dennison SE, Keuler NS, Schwarz T. Computed tomographic imaging protocol for the canine cervical and lumbar spine. Vet Radiol Ultrasound 2009;50:74–79.

34. Zamyatin AA, Hein IA, Silver MD, Nakanishi S. *Up-sampling with shift method for windmill correction*. Paper presented at Nuclear Science Symposium Conference Record, 2006. IEEE, 2006; San Diego, CA, USA.

35. Flohr TG, Schaller S, Stierstorfer K, Bruder H, Ohnesorge BM, Schoepf UJ. Multi-detector row CT systems and image-reconstruction techniques. Radiology 2005;235:756–773.

36. Mori I. Antialiasing backprojection for helical MDCT. Med Phys 2008;35:1065–1077.

37. Dalrymple NC, Prasad SR, El-Merhi FM, Chintapalli KN. Price of isotropy in multidetector CT1. Radiographics 2007;27:49–62.

38. Paulson EK, Jaffe TA, Thomas J, Harris JP, Nelson RC. MDCT of patients with acute abdominal pain: a new perspective using coronal reformations from submillimeter isotropic voxels. Am J Roentgenol 2004;183:899–906.

39. Szucs-Farkas Z, Verdun FR, von Allmen G, Mini RL, Vock P. Effect of X-ray tube parameters, iodine concentration, and patient size on image quality in pulmonary computed tomography angiography: a chest-phantom-study. Invest Radiol 2008;43:374–381.

40. Ohlerth S, Scharf G. Computed tomography in small animals—basic principles and state of the art applications. Vet J 2007;173:254–271.

41. Pappas JN, Donnelly LF, Frush DP. Reduced frequency of sedation of young children with multisection helical CT1. Radiology 2000;215:897–899.